

Controlling T_c through band structure and correlation engineering in collapsed and uncollapsed phases of iron arsenides

Swagata Acharya, Dimitar Pashov, Francois Jamet, and Mark van Schilfgaarde

King's College London, Theory and Simulation of Condensed Matter, The Strand, WC2R 2LS London, UK*

Recent observations of selective emergence (suppression) of superconductivity in the uncollapsed (collapsed) tetragonal phase of LaFe_2As_2 has rekindled interest in understanding what features of the band structure control the superconducting T_c . We show that the proximity of the narrow $\text{Fe-}d_{xy}$ state to the Fermi energy emerges as the primary factor. In the uncollapsed phase this state is at the Fermi energy, and is most strongly correlated and source of enhanced scattering in both single and two particle channels. The resulting intense and broad low energy spin fluctuations suppress magnetic ordering and simultaneously provide glue for Cooper pair formation. In the collapsed tetragonal phase, the d_{xy} state is driven far below the Fermi energy, which suppresses the low-energy scattering and blocks superconductivity. A similar source of broad spin excitation appears in uncollapsed and collapsed phases of CaFe_2As_2 . This suggests controlling coherence provides a way to engineer T_c in unconventional superconductors primarily mediated through spin fluctuations.

Through careful control of growth and annealing conditions, LaFe_2As_2 (LFA) can be grown in the tetragonal phase with markedly longer c -axis than the value in the equilibrium “collapsed” tetragonal (CT) phase ($c=11.01\text{ \AA}$). The “uncollapsed” tetragonal phase (UT) has $c=11.73\text{ \AA}$. Moreover, the UT phase is shown to superconduct at 12.1 K, while the CT phase is not a superconductor¹. A parallel phenomenon was observed in undoped CaFe_2As_2 (CFA). At room temperature, the equilibrium phase is UT, but it was recently shown that a CT phase can be induced by quenching films grown at high temperature². In this case, the undoped CT phase superconducts with $T_c=25\text{ K}$. The UT phase does not exist at low temperature because CFA undergoes a transition from tetragonal (I4/mmm) to orthorhombic (Fmmm) phase at 170 K³, with a concomitant transition to an ordered antiferromagnetic state⁴. It is also possible to induce a CT phase at low temperature by applying pressure^{5,6}: superconductivity was reported with T_c 12 K at 0.3 GPa. Taken together, these findings re-ignite the longstanding question as to whether universal band features can explain unconventional superconductivity.

Here we use a recently developed *ab initio* technique to show that there is indeed a universal feature, namely incoherence originating from the $\text{Fe-}d_{xy}$ state. By ‘incoherence’ we refer to the fuzzy spectral features and momentum-broadened spin excitation caused by enhanced single- and two-particle scattering. Superconductivity depends critically on the alignment of this state to the Fermi level. We are able to make these findings thanks to recent developments that couple (quasi-particle) self consistent GW (QSGW) with dynamical mean field theory (DMFT)^{7–10}. Merging these two state-of-the-art methods captures the effect of both strong local dynamic spin fluctuations (captured well in DMFT), and non-local dynamic correlation^{11,12} effects captured by QSGW¹³. We use QSGW and not some other form of GW , e.g. GW based on DFT. It has been well established that QSGW overcomes limitations of DFT- GW when correlations become strong (see in particular

Section 4 of Ref.¹²). On top of the DMFT self-energy, charge and spin susceptibilities are obtained from vertex functions computed from the two-particle Green’s function generated in DMFT, via the solutions of non-local Bethe Salpeter equation. Additionally, we compute the particle-particle vertex functions and solve the linearized Eliashberg equation^{9,14,15} to compute the superconducting susceptibilities and eigenvalues of superconducting gap instabilities. For CT and UT phases we use a single value for U and J (3.5 eV and 0.62 eV respectively), which we obtained from bulk FeSe (and LiFeAs) within a constrained RPA implementation following Ersoy et al.¹⁶ DMFT is performed in the Fe-3d subspace, solved using a rotationally invariant Coulomb interaction generated by these U and J . The full implementation of the four-tier process (QSGW, DMFT, BSE, and BSE-SC) is discussed in Pashov et. al.¹², and codes are available on the open source electron structure suite Questaal¹⁷. Expressions we use for the response functions are presented in Ref.⁹. Our all-electronic GW implementation was adapted from the original ecalj package¹⁸; the method and basis set are described in detail in Ref.¹². For the one-body part a k -mesh of $12 \times 12 \times 12$ was used; to compute the (much more weakly k -dependent) self-energy, we used a mesh of $6 \times 6 \times 6$ divisions, employing the tetrahedron method for the susceptibility.

We perform calculations in the tetragonal phases of LFA and CFA; in the CT phase (CT-LFA and CT-CFA) and the corresponding UT phase (UT-LFA and UT-CFA). Structural parameters for each phase are given in the SM, Table 1. The DMFT self-energy, spin and charge susceptibilities, and finally the superconducting instability are computed as a function of temperature. CT-QMC samples more electronic diagrams at reduced temperature and provides insights into the emerging coherence/incoherence in single- and two-particle instabilities; however, it cannot provide knowledge about entrant structural (or structural+magnetic) transitions. On the other hand, it can tell us what would happen if the structural+magnetic transition could be suppressed

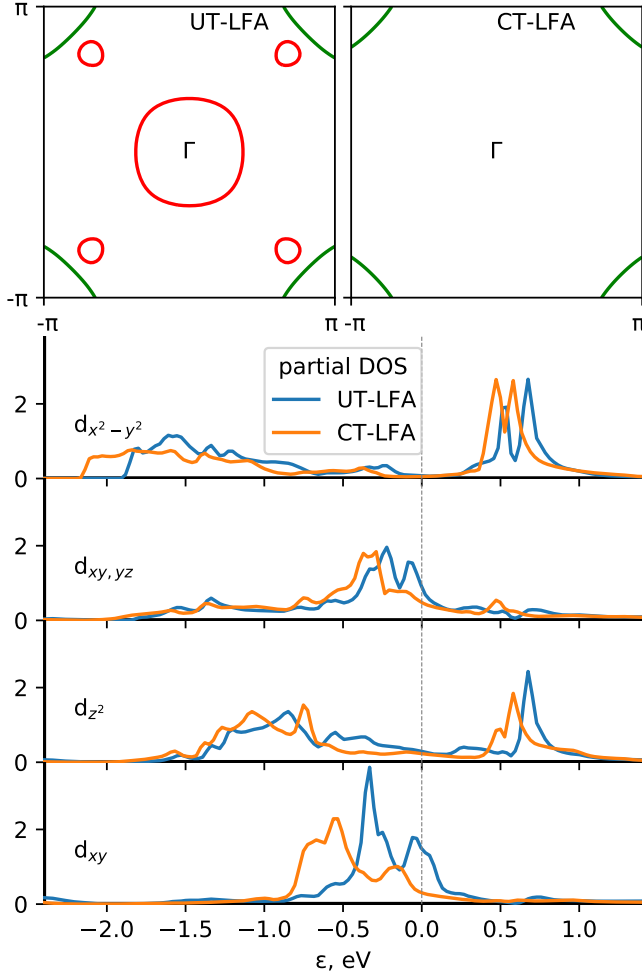


FIG. 1. Fermi surface in the $k_z=0$ plane for UT and CT-LFA phases. In the UT phase, the circular pocket around Γ has Fe- d_{xy} character, while chickpea shaped pockets are of Fe- $d_{xz,yz}$ character. These pockets disappear in the CT phase where superconductivity is absent. Simultaneously, the effective band width W of the Fe-3d manifold significantly increases in CT phase (~ 4 eV, in the UT phase $W \sim 2.4$ eV, leading to larger electronic itineracy. Also shown is the partial local density of states projected onto the Fe-3d orbitals. The bandwidth W of narrow d_{xy} states gets further narrowed in UT-LFA phase to mark enhancement in effective correlation ($\frac{U}{W}$), where U is the Hubbard parameter.

($T_N=170$ K in CFA), and we can estimate T_c in the hypothetical UT phase of undoped CFA below T_N .

In brief, we find that the CT-LFA has no superconducting instability, while UT, CT-CFA and UT-LFA are all predicted to be superconducting. All of these findings are consistent with experiment. In the experimentally known cases where the systems do superconduct (UT-LFA and CT-CFA), it appears our estimated T_c 's are a factor of two to three times larger than the experimental T_c . A similar discrepancy is observed in estimation of T_c in doped single-band Hubbard model¹⁴, where it sources from the local approximations of DMFT and

needs a better momentum dependent vertex to circumvent this¹⁹. Apart from a constant scaling, all of these findings are consistent with experiment. Moreover, we find that the hypothetical UT-CFA phase can have the highest T_c of all. We conclude that UT-CFA would be superconducting if it did not make a transition to an antiferromagnetically ordered state. The superior quality of the QSGW bath combined with nonperturbative DMFT has been shown to possess a high degree of predictive power in one- and two-particle spectral functions^{7-9,12} and as in other cases we are able to replicate the experimental observations of spectral functions, including a reasonable estimate for T_c . The remainder of the paper uses this machinery to explain what the origins of superconductivity are.

The three systems predicted to have non-negligible T_c (CT-CFA, UT-LFA, UT-CFA) have two things in common. First, the Fe- d_{xy} state contributes to the hole pocket around the Γ point (Fermi surface is shown in Fig. 1; see also the blue band in Fig. 2). Second, the imaginary part of the spin susceptibility $\text{Im} \chi(q, \omega)$ has intense peaks centered at $\mathbf{q}=(\frac{1}{2}, \frac{1}{2}, 0)2\pi/a$, in the energy window (2,25) meV. The latter is a consequence of the former: low-energy spin-flip transitions involving d_{xy} are accessible, which give rise to strong peaks in $\text{Im} \chi(q, \omega)$ around the antiferromagnetic nesting vector $\mathbf{q}^{\text{AFM}}=(\pi/a, \pi/a, 0)$. $\text{Im} \chi(q, \omega)$ is diffused in \mathbf{q} around \mathbf{q}^{AFM} . This broadening in momentum space suppresses antiferromagnetism to allow superconductivity to form. CT-LFA is the only one of the four systems that has negli-

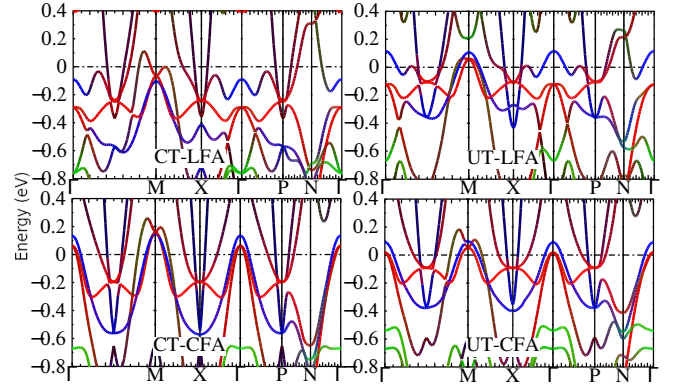


FIG. 2. Color-weighted electronic QSGW band structures in LFA (top) and CFA (bottom). CT (UT) phases are displayed on the left (right). All t_{2g} Fe states (d_{xy} in blue, $d_{xz,yz}$ in red) are in close proximity to the Fermi energy, while the Fe- d_{eg} states (depicted in green) are somewhat below. In the CT phase of LFA, the d_{xy} state is pushed below E_F , eliminating the hole pocket at Γ and suppressing T_c .

gible instability to superconductivity. In CT-LFA the Fe- d_{xy} state is pushed down (Fig. 2). As a consequence the peak in $\text{Im} \chi(\mathbf{q}^{\text{AFM}}, \omega)$ occurs at a much higher energy — too high to provide the low-energy glue for Cooper pairs. Also appearing is a pronounced dispersive paramagnon branch around $q=0$. This branch is present in all four

systems, but it is strongest in CT-LFA. Nevertheless the *ab initio* calculations predict no superconductivity. This establishes that the paramagnon branch contributes little to the glue for superconductivity in these 122-As based compounds.

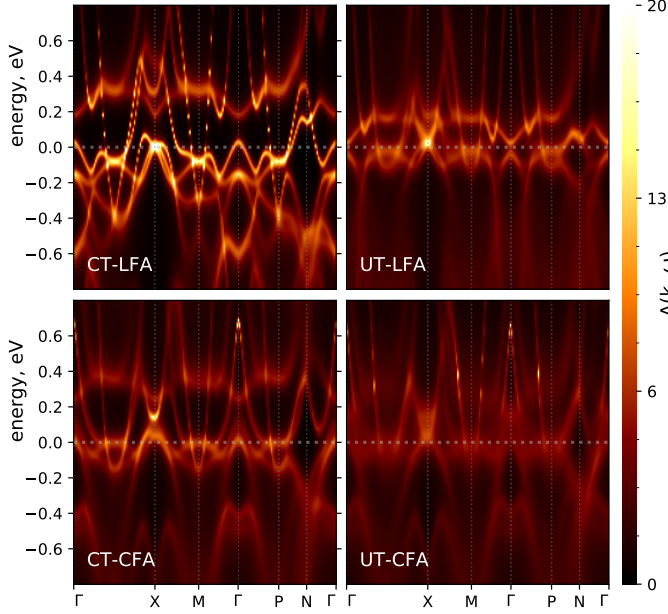


FIG. 3. Single-particle correlated QSGW+DMFT electronic spectral functions $A(q, \omega)$ for CT and UT phases of LF and CFA along high-symmetry lines. The UT-CFA phase is most incoherent, while the CT-LFA phase is most coherent. The presence (absence) of Fe- d_{xy} state at Fermi energy appears to be the primary criterion for incoherent (coherent) spectral features.

Reducing the c -axis in LFA phase pushes d_{xy} below the Fermi energy E_F (top left panel, Fig. 2); the remaining hole pocket at Γ is without d_{xy} character (see Fig. 1). Quasi-particles in CT-LFA are much more coherent (see Fig. 3) with small scattering rate Γ (extracted from the imaginary part of the self-energy at $\omega \rightarrow 0$) and large quasi-particle weights Z relative to the other cases (see SM Table 2 for the orbitally resolved numbers). This further confirms that the CT-LFA phase is itinerant with small correlation, using U/W as a measure. When the d_{xy} state crosses E_F , single-particle spectral functions $A(q, \omega)$ become markedly incoherent. This originates from enhanced single-particle scattering induced by local moment fluctuations within DMFT and suppressed orbitally resolved Z (SM Table 2). In the superconducting cases the d_{xy} orbital character is the primary source of incoherence with high scattering rate ($\Gamma > 60$ meV) and quasi-particle weight as low as ~ 0.4 .

The peak in $\text{Im}\chi(\mathbf{q}^{\text{AFM}}, \omega)$ can be observed in almost all iron based superconductors^{15,20}. However, what varies significantly over various systems is the dispersion of the branches. The less itinerant the system is, the smaller dispersion in $\text{Im}\chi(q, \omega)$ (and typical spin exchange scale $J \sim t^2/U$), and it is more strongly corre-

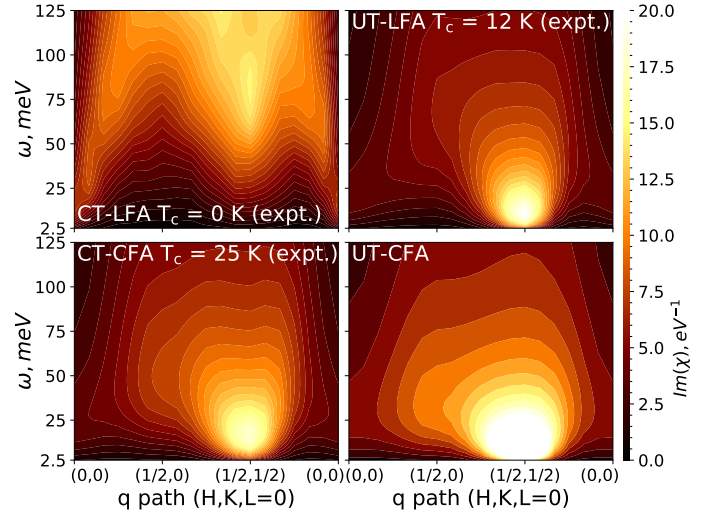


FIG. 4. The energy and momentum resolved spin susceptibility $\text{Im}\chi(q, \omega)$ (in the top panel from left to right) shown for the CT and UT phases respectively. The q -path ($H, K, L=0$) is chosen along $(0,0) - (\frac{1}{2}, 0) - (\frac{1}{2}, \frac{1}{2}) - (0,0)$ in the Brillouin zone corresponding to the two-Fe atom unit cell. The intensity in the CT phase is artificially multiplied by five to bring excitations for CT and UT phases to the same scale.

lated.

In the UT-LFA phase, $\text{Im}\chi(q, \omega)$ has a dispersive magnon branch extending to ~ 70 meV. As can be observed in Fig. 9, both the branch and the low-energy peak at $(\frac{1}{2}, \frac{1}{2}, 0)$ are significantly broad. The dispersion is significantly smaller than in undoped BaFe_2As_2 (BFA)²¹, dispersion survives up to 200 meV at $(\frac{1}{2}, 0, 0)$. This suppression of branches and concomitant broadening suggests that UT-LFA is more correlated than BFA. In contrast with UT-LFA, CT-LFA has Stoner like continuum of spin excitations (in the figure the intensity is scaled by a factor of five to make it similar to the UT phase) without any well defined low energy peak. Similar spin excitations can be observed in the phosphorus compounds (BaFe_2P_2 , LiFeP) where the system either does not superconduct or T_c is fairly low (when it does)¹⁵. These are among the most itinerant systems of all iron based superconductors and both the quasi-particle and spin excitations are band like. In both the phases we find weak to no q_z -dispersion of the susceptibilities, making the spin fluctuations effectively two dimensional.

In Fig. 5 we compare $\text{Im}\chi(q, \omega)$ at $(\frac{1}{2}, \frac{1}{2}, 0)$ for four candidates. The UT-CFA has most intense low energy peak followed by CT-CFA and UT-LFA. Low energy spin excitations for CT-LFA is gapped at $(\frac{1}{2}, \frac{1}{2}, 0)$. Further, we take three energy cuts of $\text{Im}\chi(q, \omega)$ at $\omega = 15, 30, 60$ meV along the path $(H, K, L=0) = (0,0) - (\frac{1}{2}, 0) - (\frac{1}{2}, \frac{1}{2}) - (0,0)$. At 15 meV, the UT-CFA peak is significantly stronger than the rest; CT-LFA has weak uniform spin excitation at $q=0$, and is almost entirely suppressed at $(\frac{1}{2}, \frac{1}{2}, 0)$. It appears that an intense low energy peak which is simultaneously broadened in momentum space provides max-

imum favorable glue for superconducting ordering. For higher energy $\omega=30$ and 60 meV, cuts the sharp difference between UT-CFA and others start to diminish and the spin excitations for all systems become broad and incoherent and nearly comparable. CT-LFA shows a clear two-peak structure associated with the high energy paramagnon branch and it disperses to ~ 500 meV (see SM). The eigenvalues and eigenfunctions of superconducting

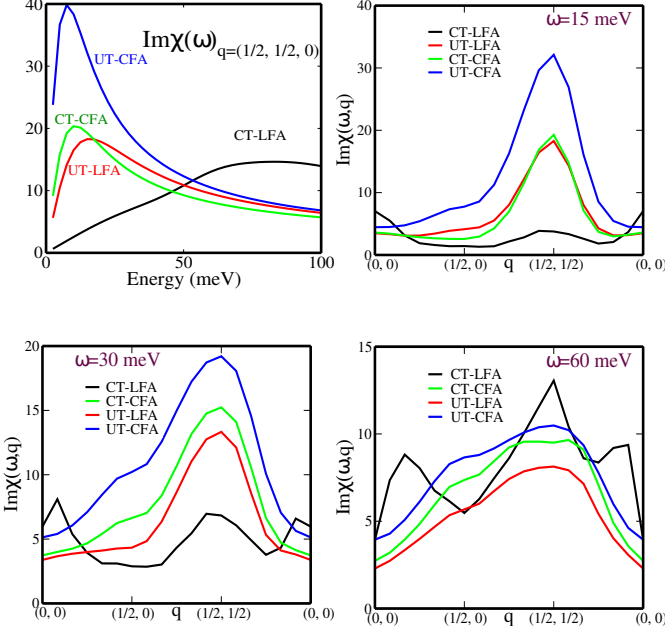


FIG. 5. The low energy behavior of $\text{Im}\chi(q, \omega)$ is shown for four candidates at $q=(\frac{1}{2}, \frac{1}{2}, 0)$. The more intense the peak is, higher is the T_c . Three different energy cuts at 15, 30 and 60 meV for $\text{Im}\chi(q, \omega)$ are resolved along the q -path $(H, K, L=0)=(0, 0)-(\frac{1}{2}, 0)-(\frac{1}{2}, \frac{1}{2})-(0, 0)$ to stress the low-energy concentration of glue in the superconducting phases. (The intensity of CT-LFA peak is artificially multiplied by five to bring excitations for CT and UT phases to the same scale)

susceptibilities, superconducting pairing symmetries can not be extracted from the spin dynamics alone. We compute the full two particle scattering amplitude in the particle-particle channel within our DMFT framework, and we solve Eliashberg equations in the BCS low energy approximation^{9,14,15}. We resolve our eigenfunctions of the gap equation into different inter- and intra-orbital channels, and observe the trend in the leading eigenvalues with temperature in both CT and UT phases. We observe that there are two dominant eigenvalues of the gap equation. The eigenvalues increase with decreasing T in the UT-LFA, UT-CFA and CT-CFA, while they are vanishingly small (at least one order of magnitude smaller than the UT phase) and (in the CT-LFA phase) insensitive to T . The corresponding eigenfunctions in the UT-LFA phase have extended s -wave (leading eigenfunction Δ_1 for eigenvalue λ_1) and $d_{x^2-y^2}$ (lagging eigenfunction Δ_2 for eigenvalue λ_2) characters (see Fig. 6). We also find that these instabilities are primarily in the intra-

orbital d_{xy} - d_{xy} channel and the inter-orbital components are negligible. In both the UT and CT-CFA phases the only instability appears to be of extended s -wave nature. We track the temperature at which the superconducting susceptibility diverges (the leading eigenvalue approaches one) to estimate T_c (see Fig. 6). We find that the pairing vertex Γ rises steeply with lowering temperatures and the leading eigenvalue λ follows the temperature dependence of Γ (see SM). Suppression of the charge component of Γ leads to no qualitative change to the temperature dependence of λ and only weakly changes its magnitude (see SM). Our results suggest that T_c is directly proportional to the strength of the low energy peak at $(\frac{1}{2}, \frac{1}{2})$, which is further controlled by the correlations and scattering in the Fe- $3d_{xy}$ state.

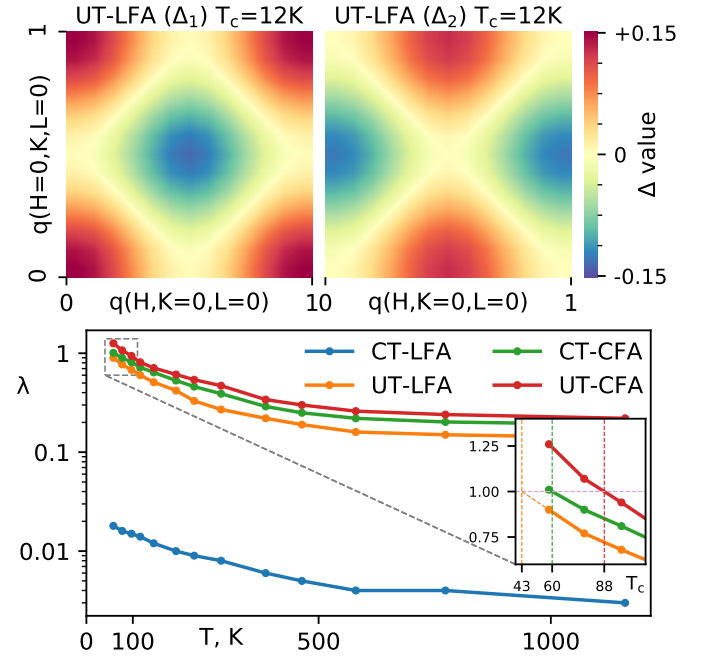


FIG. 6. The superconducting instability is absent in the CT-LFA phase. The superconducting instability corresponding to the leading (λ_1) and lagging (λ_2) eigenvalues of the solutions to the linearized Eliashberg equations, $\Delta(q, \omega=0)$ are shown for the UT-LFA phase. The evolution of the leading eigenvalue as a function of temperature is shown for CT-CFA, UT-CFA and UT-LFA in the bottom panel. In inset we zoom into the low temperature part of the curves to show the estimated T_c 's.

To conclude, we establish the interplay between the band structure and correlations that lead to emergence (suppression) of superconductivity in the UT-LFA (CT-LFA) phase. We establish a direct correspondence between the proximity of the d_{xy} state to the Fermi energy, and show that it contributes to enhanced low energy scattering and significantly incoherent quasi-particles. Incoherence affects two-particle features: the spin susceptibilities also show broad and intense low energy spin fluctuations centered at $(\frac{1}{2}, \frac{1}{2})$. As the phase is quenched, in

CT-LFA, d_{xy} is pushed below E_F , which causes coherent spectral features to emerge with a broad continuum of spin excitations. These do not provide glue conducive for Cooper pair formation. Our conclusions find further validation in our calculations in UT and CT phases in CFA. UT-CFA was found to have the most intense low energy susceptibility peak among the four candidates and is predicted to have the highest, were the superconducting instability not suppressed by entrant first order structural transition.

variants	a (Å)	c(Å)	h_{se}
CT-LFA ¹	4.0035	11.0144	0.3589
UT-LFA ¹	3.9376	11.7317	0.3657
CT-CFA ²	3.873	11.5647	0.3657
UT-CFA ⁴	3.8915	11.69	0.372

TABLE I. Structural parameters, pnictogen height h_{as} as a fraction of c entering as inputs for CT-LFA, UT-LFA, CT-CFA, UT-CFA.

variants	U (eV)	J (eV)
CT-LFA ¹	3.9	0.72
UT-LFA ¹	3.88	0.72
CT-CFA ²	3.97	0.73
UT-CFA ⁴	3.99	0.73

TABLE II. Hubbard parameters U, J computed using QSGW + C-RPA for CT-LFA, UT-LFA, CT-CFA, UT-CFA.

SUPPLEMENTAL MATERIAL

CRYSTAL STRUCTURE, QUASIPARTICLE PROPERTIES AND SUSCEPTIBILITIES

In this supplemental material, we show we list the input structural parameters for our calculations, and the orbitally resolved quasi-particle weight and scattering rates in different compounds, as extracted from QSGW+DMFT. We also show the $\text{Im}\chi(q, \omega)$ upto 500 meV to demonstrate the itinerant character of spin excitations in CT-LFA.

Note on U and J

We performed calculations with U and J taken from constrained RPA values for the FeSe and LiFeAs. Subsequent constrained RPA calculations on the pnictide considered here (Table II above) indicate that they are about 15% larger than the values we used. with the change in U and J uniform across all four compounds. Also the ratio $J/U \sim 0.17$ is essentially unchanged. While correlations should increase, the conclusions will not change since the adjustment is small and uniform, and we cannot justify repeating the calculations, in light of the high cost of these calculations.

This work was supported by the Simons Many-Electron Collaboration. We acknowledge PRACE for awarding us access to SuperMUC at GCS@LRZ, Germany, STFC Scientific Computing Department's SCARF cluster, Cambridge Tier-2 system operated by the University of Cambridge Research Computing Service (www.hpc.cam.ac.uk) funded by EPSRC Tier-2 capital grant EP/P020259/1.

variants	$\Gamma_{x^2-y^2}$	$Z_{x^2-y^2}$	$\Gamma_{xz,yz}$	$Z_{xz,yz}$	Γ_{z^2}	Z_{z^2}	Γ_{xy}	Z_{xy}
CT-LFA	14	0.67	18	0.63	12	0.67	21	0.72
UT-LFA	28	0.54	60	0.54	32	0.5	67	0.49
UT-CFA	20	0.50	45	0.43	23	0.47	49	0.44
CT-CFA	26	0.53	50	0.45	24	0.50	47	0.47

TABLE III. Quasi-particle renormalization factor (Z), single-particle scattering rate (γ) for CT and UT phases.

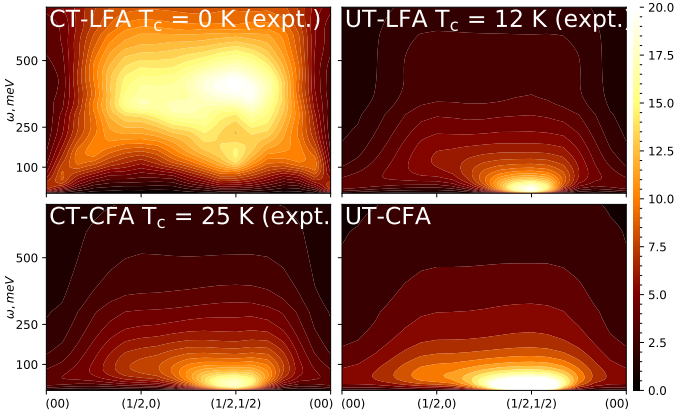


FIG. 7. The energy and momentum resolved spin susceptibility $\text{Im}\chi(q, \omega)$ (in the top panel from left to right) shown for the CT and UT phases respectively over much higher energies to stress the absence of low energy glue in CT-LFA phase, and its nearly band like spin excitation character. The intensity in the CT phase is artificially multiplied by five to bring excitations for CT and UT phases to the same scale.

A note on T_c estimation

We compute the pairing eigenvalues by solving the linearized Eliashberg equation at different temperatures in the normal phase. The temperature at which the leading eigenvalue becomes one, is where the particle-particle ladder sum (superconducting pairing susceptibility) diverges and corresponds to the T_c for that material (the entire method is detailed in our recent work⁹ and Park's thesis¹⁴). The local three frequency, orbital dependent vertex functions for solving these linearized Eliashberg equations are computed from CT-QMC. CT-QMC is quantum monte carlo based finite temperature solver. It is fairly expensive to sample the desired vertex functions from CT-QMC, for example, at 300 K, we sample the CT-QMC vertex by launching the calculation on 40,000 cores for 4 hours.

The superconducting pairing susceptibility χ^{p-p} is computed by dressing the non-local pairing polarization bubble $\chi^{0,p-p}(\mathbf{k}, i\nu)$ with the pairing vertex $\Gamma^{irr,p-p}$ using the Bethe-Salpeter equation in the particle-particle channel.

$$\chi^{p-p} = \chi^{0,p-p} \cdot [\mathbf{1} + \Gamma^{irr,p-p} \cdot \chi^{0,p-p}]^{-1} \quad (1)$$

$\Gamma^{irr,p-p}$ in the singlet (s) channel is obtained from the magnetic (spin) and density (charge) particle-hole reducible vertices by

$$\begin{aligned} \Gamma_{\alpha_2, \alpha_4}^{irr,p-p,s}(\mathbf{k}, i\nu, \mathbf{k}', i\nu') &= \Gamma_{\alpha_2, \alpha_4}^{f-irr}(\mathbf{k}, i\nu, \mathbf{k}', i\nu') \\ &+ \frac{1}{2} [\frac{3}{2} \tilde{\Gamma}^{p-h,(m)}]_{\alpha_1, \alpha_3} \\ &- \frac{1}{2} \tilde{\Gamma}^{p-h,(d)}_{\alpha_2, \alpha_3}(\mathbf{k}, i\nu, -i\nu')_{\mathbf{k}'-\mathbf{k}, i\nu'-i\nu} \\ &+ \frac{1}{2} [\frac{3}{2} \tilde{\Gamma}^{p-h,(m)}]_{\alpha_1, \alpha_3} \\ &- \frac{1}{2} \tilde{\Gamma}^{p-h,(d)}_{\alpha_4, \alpha_3}(\mathbf{k}, i\nu, -i\nu')_{-\mathbf{k}'-\mathbf{k}, -i\nu'-i\nu} \end{aligned} \quad (2)$$

Finally, χ^{p-p} can be represented in terms of eigenvalues λ and eigenfunctions ϕ^λ of the Hermitian particle-particle pairing matrix.

$$\chi^{p-p}(k, k') = \sum_{\lambda} \frac{1}{1 - \lambda} \cdot (\sqrt{\chi^{0,p-p}(k)} \cdot \phi^\lambda(k)) \cdot (\sqrt{\chi^{0,p-p}(k')} \cdot \phi^\lambda(k')) \quad (3)$$

The pairing susceptibility diverges when the leading eigenvalue approaches unity. When the particle-particle ladder sum $\chi^{p-p} = ((\chi^{0,p-p})^{-1} - \Gamma^{p-p})^{-1}$ diverges, the normal state becomes unstable towards superconductivity. In a temperature dependent calculation this corresponds to the T_c where the leading eigenvalue of the matrix $\Gamma^{p-p}\chi^0$ reaches one (as shown in Eqn. (3)). The eigenvector corresponding to the leading eigenvalue λ gives the symmetry of the superconducting order parameter $\Delta_{\alpha,\beta}(k, \nu)$. In an ideal scenario we need to solve the eigenvalue problem of the following matrix;

$$-K_B T \sum_{k', \nu', \alpha', \beta', \gamma, \delta} \gamma^{p-p,s}(\alpha\beta k\nu; \alpha'\beta' k'\nu') \chi_{\alpha'\beta'\gamma\delta}^{0,p-p}(k', \nu') \Delta(\gamma\delta)(k', \nu') = \lambda \Delta_{\alpha,\beta}(k, \nu) \quad (4)$$

The matrix that needs to be diagonalized has a size $(norb^2 * nomega * nkp) * (norb^2 * nomega * nkp)$. In case of our materials, we find that even at $\beta=20$, which is roughly $T = 580$ K, the matrix size that we need to diagonalize is of the size $(norb=5, nomega=200, nkp=1000)$ size $(25*200*1000)*(25*200*1000)$. So we employ BCS low energy approximation to diagonalize the matrices at different temperatures and extract the eigenvalue spectrum. The BCS approximation amounts to using the Γ^{p-p} strictly from the lowest energy ($\nu = 0^+$, $\nu' = 0^+$, $\omega=0$). However, Γ^{p-p} contains all relevant momentum and orbital structure, and bubble contains information from all energies, momentum and orbitals. This appears to be reasonable approximation as the vertex contains essential features of superconductivity which is a low energy phenomenon. Additionally the pairing vertex also shows the essential temperature dependent enhancement that is prerequisite to Cooper pairing. We project the computed bubble and vertex functions on to the leading superconducting pairing symmetry channel $\Delta^{k \sim (cosk_x + cosk_y)}$ and show their temperature dependent behaviour.

$$\bar{\Gamma} = \frac{\sum_{k,k'} \Delta^k \Gamma(k, k') \Delta^{k'}}{\sum_k (\Delta(k))^2} \quad (5)$$

$$\bar{\chi}^0 = \frac{\sum_{k,k'} \Delta^k \chi^0(k, k') \Delta^{k'}}{\sum_k (\Delta(k))^2} \quad (6)$$

Further, we suppress the charge (density) component of the Γ^{p-p} to show that the eigenvalues (λ^{-c}) only get very weakly affected. This is in complete consistency

with what we show in the main paper that the superconducting instability is in one-to-one correspondence with the spin instability and the pairing is primarily mediated via spin fluctuations.

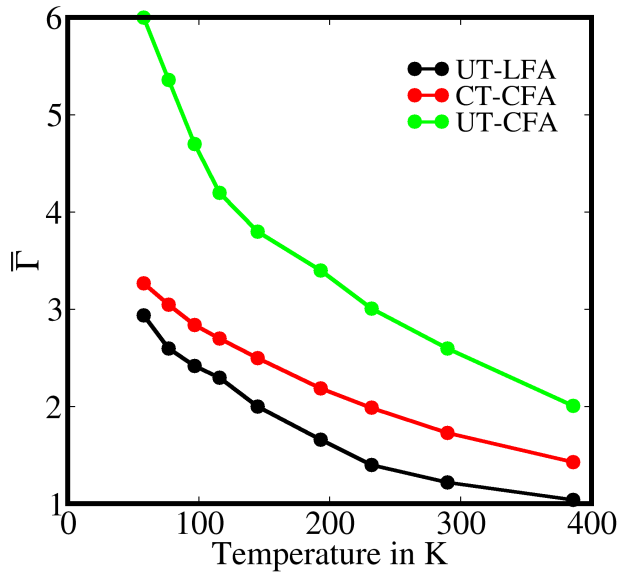
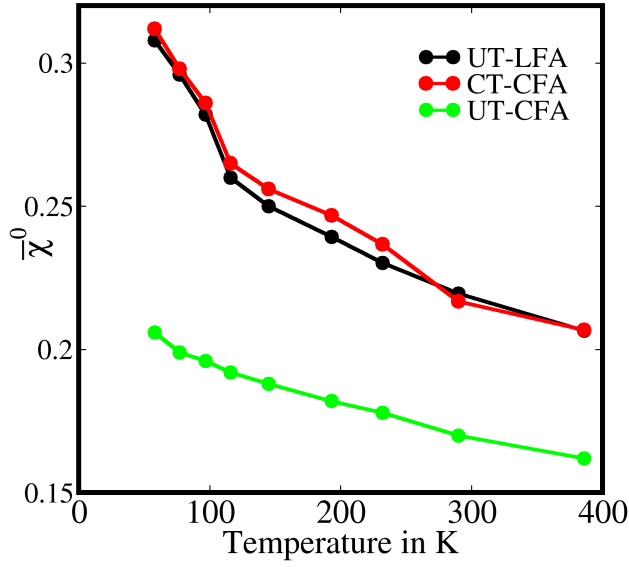


FIG. 8. The particle-particle bubble $\bar{\chi}^0$ and the particle-particle interaction vertex $\bar{\Gamma}$ (projected onto the leading pairing symmetry channel) are plotted as functions of temperature. The leading eigenvalue of the Eliashberg gap equation λ follows primarily the steep rise in $\bar{\Gamma}$ with lowering temperatures.

* swagata.acharya@kcl.ac.uk

¹ A. Iyo, S. Ishida, H. Fujihisa, Y. Gotoh, I. Hase,

Y. Yoshida, H. Eisaki, and K. Kawashima, *The Journal of Physical Chemistry Letters* **10**, 1018 (2019),

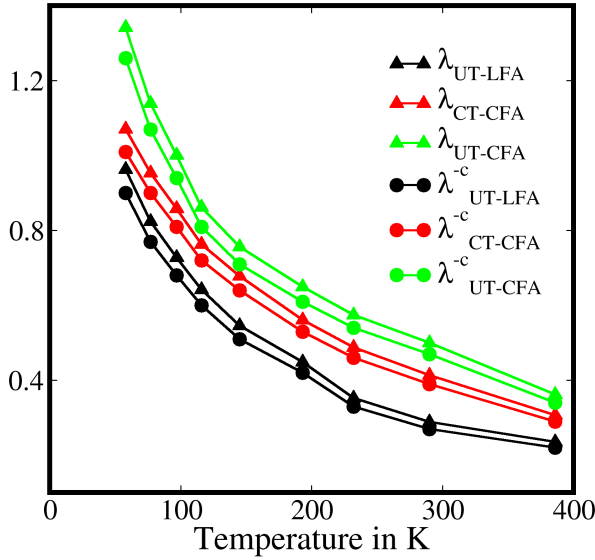


FIG. 9. The leading eigenvalue of the Eliashberg gap equation λ is shown to get very weakly affected once the charge component of the pairing interaction vertex Γ is suppressed (see Eqn.(2)). The original λ with both spin and charge components kept in the vertex and the one without the charge component λ^{-c} have similar temperature dependence.

<https://doi.org/10.1021/acs.jpcllett.9b00321>.

- ² D.-Y. Chen, J. Yu, B.-B. Ruan, Q. Guo, L. Zhang, Q.-G. Mu, X.-C. Wang, B.-J. Pan, G.-F. Chen, and Z.-A. Ren, Chinese Physics Letters **33**, 067402 (2016).
- ³ Q. Huang, Y. Qiu, W. Bao, M. Green, J. Lynn, Y. Gasparovic, T. Wu, G. Wu, and X. Chen, Physical Review Letters **101**, 257003 (2008).
- ⁴ N. Ni, S. Nandi, A. Kreyssig, A. Goldman, E. Mun, S. BudKo, and P. Canfield, Physical Review B **78**, 014523 (2008).

- ⁵ M. S. Torikachvili, S. L. Bud'ko, N. Ni, and P. C. Canfield, Phys. Rev. Lett. **101**, 057006 (2008).
- ⁶ A. Kreyssig, M. A. Green, Y. Lee, G. D. Samolyuk, P. Zajdel, J. W. Lynn, S. L. Bud'ko, M. S. Torikachvili, N. Ni, S. Nandi, J. B. Leão, S. J. Poulton, D. N. Argyriou, B. N. Harmon, R. J. McQueeney, P. C. Canfield, and A. I. Goldman, Phys. Rev. B **78**, 184517 (2008).
- ⁷ L. Sponza, P. Pisanti, A. Vishina, D. Pashov, C. Weber, M. van Schilfgaarde, S. Acharya, J. Vidal, and G. Kotliar, Phys. Rev. B **95**, 041112 (2017).
- ⁸ S. Acharya, D. Dey, T. Maitra, and A. Taraphder, Journal of Physics Communications **2**, 075004 (2018).
- ⁹ S. Acharya, D. Pashov, C. Weber, H. Park, L. Sponza, and M. Van Schilfgaarde, Communications Physics **2**, 1 (2019).
- ¹⁰ E. Baldini, M. A. Sentef, S. Acharya, T. Brumme, E. Sheveleva, F. Lyzwa, E. Pomjakushina, C. Bernhard, M. van Schilfgaarde, F. Carbone, A. Rubio, and C. Weber, Proceedings of the National Academy of Sciences (2020), 10.1073/pnas.1919451117, <https://www.pnas.org/content/early/2020/03/10/1919451117.full.pdf>.
- ¹¹ J. Tomczak, P. Liu, A. Toschi, G. Kresse, and K. Held, The European Physical Journal Special Topics **226**, 2565 (2017).
- ¹² D. Pashov, S. Acharya, W. R. Lambrecht, J. Jackson, K. D. Belashchenko, A. Chantis, F. Jamet, and M. van Schilfgaarde, Computer Physics Communications **249**, 107065 (2020).
- ¹³ T. Kotani, M. van Schilfgaarde, and S. V. Faleev, Phys. Rev. B **76**, 165106 (2007).
- ¹⁴ H. Park, *The study of two-particle response functions in strongly correlated electron systems within the dynamical mean field theory*, Ph.D. thesis, Rutgers University-Graduate School-New Brunswick (2011).
- ¹⁵ Z. Yin, K. Haule, and G. Kotliar, Nature Physics **10**, 845 (2014).
- ¹⁶ E. Şaşıoğlu, C. Friedrich, and S. Blügel, Phys. Rev. B **83**, 121101 (2011).
- ¹⁷ "Questaal website," <https://www.questaal.org>.
- ¹⁸ "ecalj package," <https://github.com/tkotani/ecalj/>.
- ¹⁹ M. Kitatani, T. Schäfer, H. Aoki, and K. Held, Phys. Rev. B **99**, 041115 (2019).
- ²⁰ Z. Yin, K. Haule, and G. Kotliar, Nature materials **10**, 932 (2011).
- ²¹ L. W. Harriger, H. Luo, M. Liu, C. Frost, J. Hu, M. Norman, and P. Dai, Physical Review B **84**, 054544 (2011).